第 43 卷 第 5 期/2023 年 3 月/光学学报 研究论文

光学学报

# 羟基四苯咪唑衍生物的空穴和电子传输性质研究

廖帆[1]，崔小英[2]，闵春刚[2*]，任爱民[3**]

[1]昆明理工大学材料科学与工程学院，云南 昆明 650093；

[2]昆明理工大学分析测试研究中心，云南 昆明 650093；

[3]吉林大学化学学院理论化学研究所，吉林 长春 130021

**摘要** 随着有机发光二极管应用范围的扩大，对发光材料的研究逐渐增多。蓝光材料因其在色温管理和显色指数方面的重要作用，促使科学家们对效率更高、性能更好的新型蓝光材料进行了大量研究。通过(含时)密度泛函理论方法，对给电子取代基9,9-二甲基-9,10-二氢吖啶(DMAC)、三苯胺(TPA)、10H-吩噻嗪(PTZ)、10H-吩噁嗪(PXZ)、苯基咔唑(PCz)和5H-吲哚[3,2,1-de]吩嗪(InPz)双取代的羟基四苯咪唑分别进行了结构优化，并研究了其光物理性质。理论计算结果表明，TPA、DMAC、PTZ、PXZ和InPz取代的羟基四苯咪唑可作为空穴传输材料，PTZ、PXZ和InPz取代的羟基四苯咪唑可作为电子传输材料。

**关键词** 光谱学；空穴和电子传输；双取代羟基四苯咪唑衍生物；荧光；密度泛函理论

**中图分类号** O436 **文献标志码** A **DOI**：10.3788/AOS221676

## 1 引 言

近年来，有机发光二极管(OLED)技术因其在全彩平板显示和照明领域中的需求逐渐增大受到了人们的广泛关注[1-7]。一般情况下，全彩显示或白色OLED(包括固态照明)均需要红、绿、蓝三原色，特别是蓝光发射在色温管理和显色指数方面发挥着至关重要的作用[8-9]。因此，科学家们对效率更高、性能更好的新型蓝光材料进行了大量研究[10-12]。2005年，Park等[13]首次合成了一类可以发出明亮蓝光的新型咪唑基材料，用羟基取代四苯基咪唑(HPI)。X射线晶体学分析和半经验分子轨道计算表明，HPI中咪唑环上的4个苯基通过限制引起分子间振动耦合和相关非辐射弛豫的过度紧密堆积使晶体免于荧光猝灭。2019年，Kajjam等[14]合成了4种分子量较小的四苯咪唑衍生物{1,2,4,5-四苯基-1H-咪唑、2,4,5-三苯基-1-对-苯甲基-1H-咪唑、1-[3-(三氟甲基)苯基]-2,4,5-三苯基-1H-咪唑和1-[4-(三氟甲基)苯基]-2,4,5-三苯基-1H-咪唑}，并利用核磁共振技术和密度泛函理论(DFT)对其传感机理和发光性质进行了详细研究，结果表明它们都能发出明亮的蓝光。2020年，Dwivedi等[15]合成并全面表征了4种氟硼荧取代的羟基四苯咪唑衍生物，研究结果表明这些化合物对黏度具有显著的敏感性。同时，由于咪唑环周围有4个苯基，故其可以作为荧光分子转子。最近，Li等[16]用三苯胺、苯基咔唑和咔唑苯基对羟基四苯咪唑中*N*-苯基的3,5位置进行了双取代，设计并合成了3种羟基四苯基咪唑双取代衍生物。研究发现，所有器件在较低的开通电压下都能发出明亮的蓝光。此外，四苯咪唑衍生物还被成功用作荧光探针来观测硫化氢[17]、亚砷酸根离子[18]和氟离子[19]。以上研究表明，四苯咪唑相似物作为蓝光材料具有良好的应用前景，故需要对其进行进一步研究。

本文中使用常用的给电子取代基9,9-二甲基-9,10-二氢吖啶(DMAC)[20]、10H-吩噻嗪(PTZ)[21]、10H-吩噁嗪(PXZ)[22]和5H-吲哚[3,2,1-de]吩嗪(InPz)[23]对羟基四苯咪唑中*N*-苯基的3,5位置进行双取代，设计了4种羟基四苯咪唑衍生物HPI-DMAC、HPI-PTZ、HPI-PXZ和HPI-InPz，并研究了它们和两种实验已合成的衍生物HPI-TPA和HPI-PCz的电子结构及光物理性质。此外，由于含有三苯胺、咔唑等富电子基团的化合物经常被用作空穴传输材料，故又研究了这6种衍生物作为空穴和电子传输材料的可能性[24]。

## 2 计算方法

本文使用DFT和含时密度泛函理论(TDDFT)方法对6种羟基四苯咪唑衍生物进行研究，所有计算均采用Gaussian 09程序包[25]完成。

首先，为了验证泛函的准确性，采用B3LYP[26]、

**收稿日期**：2022-09-05；**修回日期**：2022-09-08；**录用日期**：2022-10-17；**网络首发日期**：2022-11-04

**基金项目**：国家自然科学基金(11764026,21473071)、云南省科技厅基础研究专项(202001AT070080)

**通信作者**：*minchungang@kust.edu.cn；**renam@jlu.edu.cn

PBE0[27]和CAM-B3LYP[28]泛函结合6-31G(d, p)基组优化了实验上已合成的HPI-TPA和HPI-PCz的基态和第一单重激发态的几何结构，并计算了吸收和发射光谱。如表1所示，无论是HPI-TPA还是HPI-PCz的吸收光谱，B3LYP和CAM-B3LYP泛函的计算结果与实验值比较均有很大的偏差，而PBE0的计算值与实验值比较接近，发射光谱值的比较表现出相同的趋势。因此，在后续的计算中均采用PBE0泛函。

表1 B3LYP、PBE0和CAM-B3LYP泛函结合6-31G(d, p)基组得到的HPI-TPA和HPI-PCz的吸收和发射光谱

Table 1 Absorption and emission spectra of HPI-TPA and HPI-PCz in experimental and theoretical calculation obtained by combining B3LYP, PBE0 and CAM-B3LYP with 6-31G(d, p) basis set unit: nm

| Derivative | Absorption spectrum | | | | Emission spectrum | | | |
|---|---|---|---|---|---|---|---|---|
| | Experiment[16] | B3LYP | PBE0 | CAM-B3LYP | Experiment[16] | B3LYP | PBE0 | CAM-B3LYP |
| HPI-TPA | 338 | 364 | 350 | 302 | 402 | 478 | 448 | 351 |
| HPI-PCz | 339 | 381 | 358 | 285 | 490 | 540 | 498 | 358 |

本文使用PBE0泛函结合6-31G(d, p)基组优化了羟基四苯咪唑衍生物的几何结构。研究表明，此泛函可以准确地预测此类有机化合物的光物理性质[29-30]。基于优化后的几何结构，电离能$I_P$、电子亲和势$E_A$、空穴抽取能$P_{HE}$、电子抽取能$P_{EE}$、空穴重组能$\lambda_{hole}$和电子重组能$\lambda_{electron}$的计算公式[31-33]为

$$I_{P,a}=E^{+}(M_{+})-E^{0}(M_{0}), \tag{1}$$

$$I_{P,v}=E^{+}(M_{0})-E^{0}(M_{0}), \tag{2}$$

$$E_{A,a}=E^{0}(M_{0})-E^{-}(M_{-}), \tag{3}$$

$$E_{A,v}=E^{0}(M_{0})-E^{-}(M_{0}), \tag{4}$$

$$P_{HE}=E^{+}(M_{+})-E^{0}(M_{+}), \tag{5}$$

$$P_{EE}=E^{0}(M_{-})-E^{-}(M_{-}), \tag{6}$$

$$\lambda_{hole}=I_{P,v}-P_{HE}, \tag{7}$$

$$\lambda_{electron}=P_{EE}-E_{A,v}, \tag{8}$$

式中：$E^{0}(M_{0})$为中性几何结构的中性分子能量；$E^{+/-}(M_{+/-})$为离子几何结构的离子(阳离子/阴离子)能量；$E^{+/-}(M_{0})$为中性几何结构的离子(阳离子/阴离子)能量；$E^{0}(M_{+/-})$为离子几何结构的中性分子能量；下标中的a和v分别表示绝热和垂直。

最后，采用TD PBE0/6-31G(d, p)方法优化了6种衍生物的激发态几何结构，并用同一方法计算了所研究分子的吸收和发射光谱。

## 3 分析与讨论

### 3.1 前线分子轨道

首先，使用PBE0/6-31G(d, p)方法优化了图1中6种羟基四苯咪唑衍生物的分子结构，并以此为基础计算了这些分子的最高占据分子轨道(HOMO)能量、最

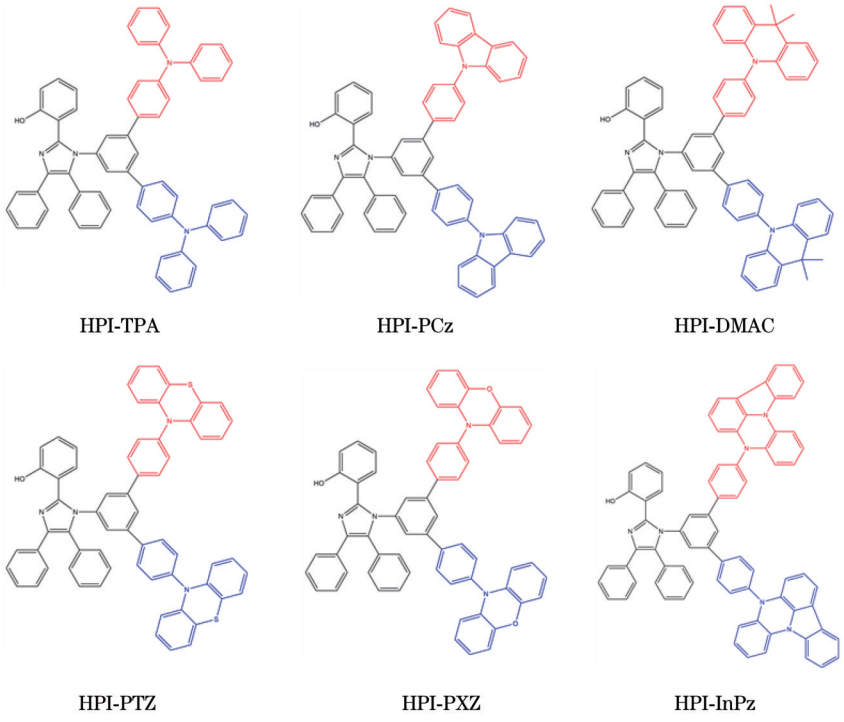


图1 设计的分子结构图

Fig. 1 Schematic diagram of designed molecular structures

低未占据分子轨道(LUMO)能量和二者的能隙$\Delta E_{\mathrm{H\text{-}L}}$。图2给出了所研究分子的Kohn-Sham前线轨道分布图。表2分析了HPI、R-up(图1中每个图右上角部分)和R-down(图1中每个图右下角部分)对前线分子轨道的贡献,其中占据分子轨道按照能量从高到低的原则表示为HOMO、HOMO−1、HOMO−2、HOMO−3、…,未占据分子轨道按照能量从低到高的原则表示为LUMO、LUMO+1、LUMO+2、LUMO+3、…。

由图2和表2可知,除HPI-PCz和HPI-DMAC外,所有羟基四苯咪唑衍生物的HOMO电子云主要位于R-down基团上,HPI和R-up对轨道基本没有贡献。在HPI-PCz中,HPI基团对HOMO的贡献为99.3%,R-up和R-down对轨道基本没有贡献。在HPI-DMAC中,R-up基团对HOMO的贡献为100.0%,HPI和R-down对轨道没有贡献。相对地,HOMO中起主要贡献的基团对LUMO的贡献均大幅减小,即从HOMO到LUMO的跃迁过程中,所有分子都存在很大的电子转移。

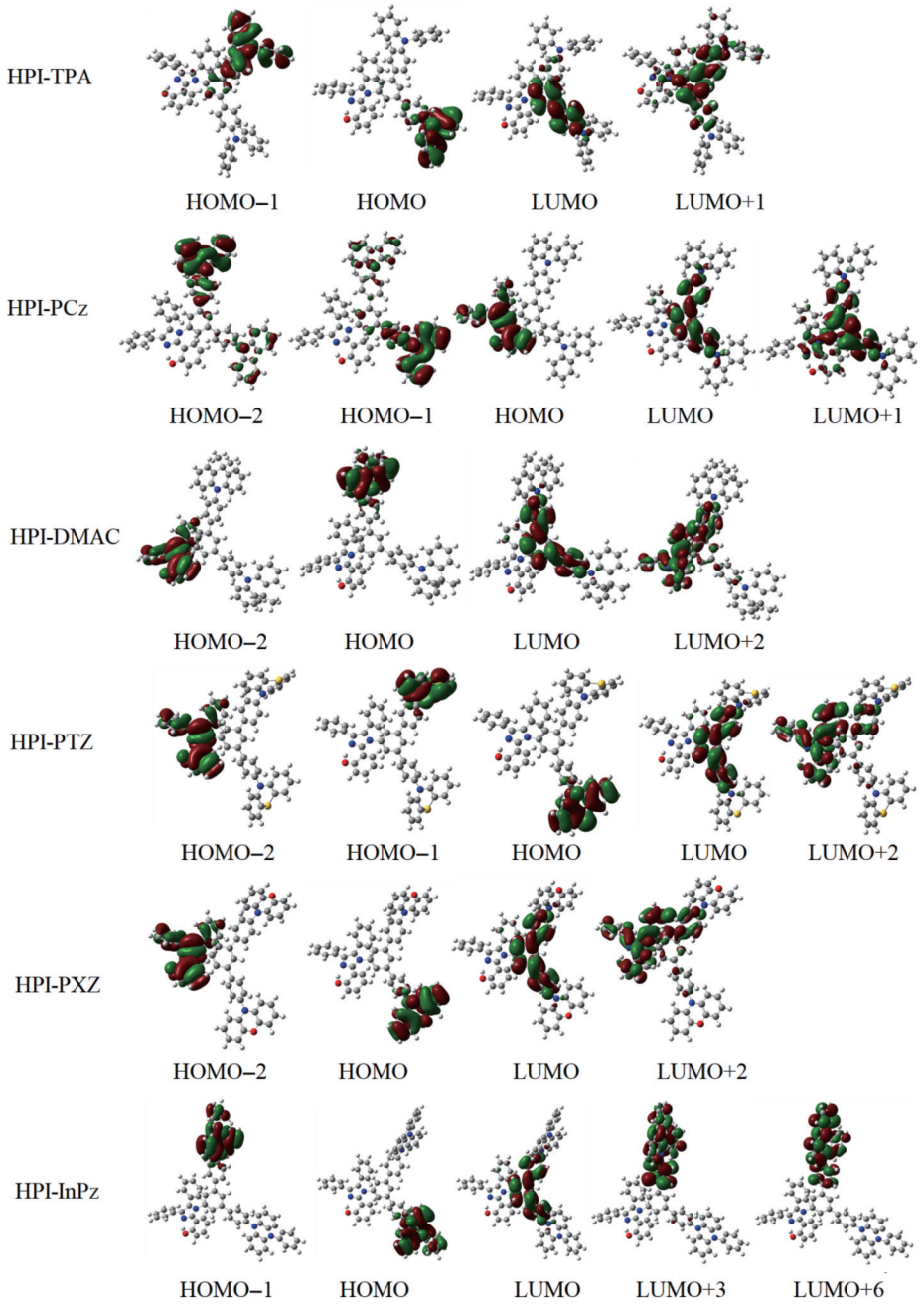


图2　PBE0/6-31G(d, p)方法预测的HPI-TPA、HPI-PCz、HPI-DMAC、HPI-PTZ、HPI-PXZ和HPI-InPz的Kohn-Sham前线轨道

Fig. 2　Kohn-Sham frontier orbitals for HPI-TPA, HPI-PCz, HPI-DMAC, HPI-PTZ, HPI-PXZ and HPI-InPz predicted by PBE0/6-31G(d, p) method

表 2 HPI-TPA、HPI-PCz、HPI-DMAC、HPI-PTZ、HPI-PXZ 和 HPI-InPz 中不同片段的电子密度对轨道的贡献

Table 2 Contribution of electron densities of different segments to orbitals in HPI-TPA, HPI-PCz, HPI-DMAC, HPI-PTZ, HPI-PXZ and HPI-InPz unit: %

| Segment | Orbital | HPI-TPA | HPI-PCz | HPI-DMAC | HPI-PTZ | HPI-PXZ | HPI-InPz |
|---|---|---|---|---|---|---|---|
| HPI | HOMO−2 | 97.0 | 2.5 | 99.8 | 99.9 | 99.8 | 99.9 |
| | HOMO−1 | 7.0 | 3.6 | 0 | 0 | 0 | 0 |
| | HOMO | 1.0 | 99.3 | 0 | 0 | 0.1 | 0 |
| | LUMO | 49.4 | 53.4 | 54.3 | 53.0 | 53.2 | 53.1 |
| | LUMO+1 | 56.2 | 58.0 | 59.7 | 56.4 | 57.6 | 56.7 |
| | LUMO+2 | 92.5 | 86.7 | 86.5 | 86.5 | 86.3 | 87.3 |
| | LUMO+3 | 18.4 | 0.1 | 67.4 | 23.1 | 18.2 | 12.0 |
| | LUMO+6 | 0.4 | 20.4 | 91.4 | 79.6 | 89.0 | 4.0 |
| R-up | HOMO−2 | 3.0 | 85.3 | 0.2 | 0.1 | 0.2 | 0 |
| | HOMO−1 | 92.8 | 11.5 | 0 | 100.0 | 100.0 | 100.0 |
| | HOMO | 0.2 | 0.5 | 100.0 | 0 | 0 | 0 |
| | LUMO | 7.9 | 23.0 | 24.5 | 24.9 | 23.8 | 23.5 |
| | LUMO+1 | 33.3 | 18.6 | 16.7 | 18.7 | 18.6 | 19.2 |
| | LUMO+2 | 6.7 | 10.6 | 10.4 | 11.2 | 10.6 | 10.1 |
| | LUMO+3 | 75.5 | 99.9 | 19.6 | 11.7 | 78.6 | 86.1 |
| | LUMO+6 | 99.6 | 47.5 | 6.0 | 15.1 | 7.5 | 95.6 |
| R-down | HOMO−2 | 0 | 12.2 | 0 | 0 | 0 | 0 |
| | HOMO−1 | 0.2 | 84.9 | 100.0 | 0 | 0 | 0 |
| | HOMO | 98.8 | 0.2 | 0 | 100.0 | 99.9 | 100.0 |
| | LUMO | 42.7 | 23.6 | 21.2 | 22.1 | 23.0 | 23.4 |
| | LUMO+1 | 10.5 | 23.4 | 23.5 | 24.8 | 23.8 | 24.1 |
| | LUMO+2 | 0.8 | 2.7 | 3.1 | 2.3 | 3.1 | 2.6 |
| | LUMO+3 | 6.1 | 0 | 13.0 | 65.2 | 3.2 | 1.9 |
| | LUMO+6 | 0 | 32.1 | 2.6 | 5.3 | 3.5 | 0.3 |

6 种双取代羟基四苯咪唑衍生物的 HOMO 能量、LUMO 能量和二者间的能隙 $\Delta E_{\text{H-L}}$ 列于表 3 中。如表 3 所示，HPI-TPA、HPI-DMAC、HPI-PTZ 的 HOMO 能量均与多功能材料 BNPB（−5.25 eV）接近[34]，而 HPI-PXZ（−4.98 eV）和 HPI-InPz（−4.81 eV）的 HOMO 能量远高于 BNPB（−5.25 eV），说明除 HPI-PCz 外，HPI-TPA、HPI-DMAC、HPI-PTZ、HPI-PXZ 和 HPI-InPz 均可作为空穴传输材料。同样地，HPI-PTZ（−1.56 eV）、HPI-PXZ（−1.56 eV）和 HPI-InPz（−1.57 eV）的 LUMO 能量与 BNPB（−1.62 eV）相当[34]，说明 HPI-PTZ、HPI-PXZ 和 HPI-InPz 同时具有较强的电子注入能力。此外，发现所研究化合物的 HOMO 和 LUMO 能隙的变窄顺序为 TPA、PCz、DMAC、PTZ、PXZ 和 InPz，说明羟基四苯咪唑衍生物的电子跃迁能力可通过取代基进行调节。

表 3 所研究化合物的 HOMO 能量、LUMO 能量和 HOMO-LUMO 能隙

Table 3 HOMO energy, LUMO energy and HOMO-LUMO energy gap of studied compounds unit: eV

| Compound | HPI-TPA | HPI-PCz | HPI-DMAC | HPI-PTZ | HPI-PXZ | HPI-InPz |
|---|---|---|---|---|---|---|
| $E_{\text{HOMO}}$ | −5.27 | −5.56 | −5.24 | −5.29 | −4.98 | −4.81 |
| $E_{\text{LUMO}}$ | −1.12 | −1.46 | −1.46 | −1.56 | −1.56 | −1.57 |
| $\Delta E_{\text{H-L}}$ | 4.15 | 4.10 | 3.78 | 3.73 | 3.42 | 3.24 |

### 3.2 电离能、电子亲和势和重组能

用 PBE0/6-31G(d, p)方法计算的电离能（$I_{\text{P,a}}$、$I_{\text{P,v}}$）和电子亲和势（$E_{\text{A,a}}$、$E_{\text{A,v}}$）值列于表 4 中。如表 4 所示，6 种羟基四苯咪唑衍生物的绝热电离能和绝热电子亲和势的顺序满足 $I_{\text{P,a,HPI-InPz}}<I_{\text{P,a,HPI-PXZ}}<I_{\text{P,a,HPI-PTZ}}<I_{\text{P,a,HPI-DMAC}}=I_{\text{P,a,HPI-TPA}}<I_{\text{P,a,HPI-PCz}}$ 和 $E_{\text{A,a,HPI-InPz}}>E_{\text{A,a,HPI-PXZ}}=E_{\text{A,a,HPI-PTZ}}>E_{\text{A,a,HPI-DMAC}}=E_{\text{A,a,HPI-PCz}}>E_{\text{A,a,HPI-TPA}}$。另外，多功能 BNPB 的电离能和电子亲和势的计算值分别为 6.18 eV 和 0.84 eV[34-35]，与其比较发现，除 HPI-PCz 以外，所有衍生物均可作为空穴传输材料。HPI-InPz、

HPI-PXZ、HPI-PT可作为电子传输材料。总之，HPI-InPz、HPI-PXZ、HPI-PTZ既可作为空穴传输材料，又可作为电子传输材料。此外，从重组能的计算结果发现，除HPI-TPA以外，所有羟基四苯咪唑衍生物的$\lambda_{hole}$均小于$\lambda_{electron}$，说明这些化合物的电子传输速率均小于空穴传输速率。

表4　所研究化合物的电离能、电子亲和势、抽取能和重组能

Table 4　Ionization potentials, electron affinities, extraction potentials and reorganization energies for studied compounds　　unit: eV

| Compound | $I_{P,v}$ | $I_{P,a}$ | $P_{HE}$ | $E_{A,v}$ | $E_{A,a}$ | $P_{EE}$ | $\lambda_{hole}$ | $\lambda_{electron}$ |
|---|---|---|---|---|---|---|---|---|
| HPI-TPA | 6.51 | 6.01 | 5.98 | 0.34 | 0.50 | 0.77 | 0.53 | 0.43 |
| HPI-PCz | 6.40 | 6.35 | 6.29 | 0.50 | 0.76 | 0.99 | 0.11 | 0.49 |
| HPI-DMAC | 6.09 | 6.01 | 5.98 | 0.49 | 0.76 | 0.99 | 0.11 | 0.50 |
| HPI-PTZ | 6.14 | 5.95 | 5.75 | 0.58 | 0.85 | 1.09 | 0.39 | 0.51 |
| HPI-PXZ | 5.87 | 5.81 | 5.76 | 0.58 | 0.85 | 1.09 | 0.11 | 0.51 |
| HPI-InPz | 5.60 | 5.55 | 5.49 | 0.61 | 0.87 | 1.11 | 0.11 | 0.50 |

### 3.3　电子吸收和发射光谱

表5列出了6种衍生物的吸收光谱、振子强度$f$和主要跃迁组成，其中$S_n$表示分子的单重态，下标$n$代表单重态能级的等级，如$S_0$表示基态，$S_1$表示第一激发单重态，$S_2$表示第二激发单重态，依次类推。高斯函数拟合的吸收光谱曲线如图3所示。如表5所示，除HPI-TPA外，其他5种羟基四苯咪唑衍生物的$S_0\rightarrow S_1$跃迁所对应的振子强度很小，是禁阻的。HPI-PCz的最大吸收峰处于340 nm处，所对应的跃迁是$S_0\rightarrow S_2$。HPI-DMAC和HPI-PTZ的最大吸收峰分别位于309 nm和310 nm处，所对应的跃迁是$S_0\rightarrow S_{10}$。HPI-PXZ和HPI-InPz最大振子强度所对应的跃迁分别是$S_0\rightarrow S_{14}$和$S_0\rightarrow S_9$。此外，HPI-TPA和HPI-PCz的最大吸收光谱与实验相比仅分别红移了12 nm和1 nm，说明TD PBE0/6-31G(d, p)得出的结果是完全可信的。

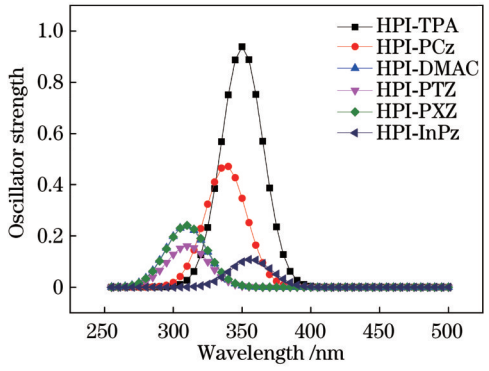


图3　高斯函数拟合的吸收光谱

Fig. 3　Absorption spectra simulated by Gaussian function

基于优化的激发态几何结构，用TD PBE0/6-31G(d,p)方法计算了6种双取代羟基四苯咪唑衍生物的发射光谱。如表6所示，因为HPI-TPA和HPI-PCz发射光谱的实验值是在甲苯中得到的，所以先计算了它们在甲苯中的发射光谱，与实验值比较发现，HPI-TPA红移了21 nm[PBE0/6-31G(d, p)方法在甲苯中计算的发射光谱峰值在423 nm处]、HPI-PCz蓝移了28 nm[PBE0/6-31G(d, p)方法在甲苯中计算的发射光谱峰值在462 nm处]，这进一步证实了所使用方法的可靠性。此外，除HPI-TPA和HPI-PCz外，其他衍生物发射光谱所对应的跃迁均是禁阻的。

## 4　结　　论

用TD PBE0/6-31G(d, p)方法研究了6种双取代羟基四苯咪唑衍生物的光电性质。计算结果表明，从HOMO到LUMO的跃迁过程中，所有分子都存在很大的电子转移。HPI-PTZ、HPI-PXZ和HPI-InPz具有较强的空穴注入能力的同时，也具有较强的电子注入能力。HOMO和LUMO能隙沿着TPA、PCz、DMAC、PTZ、PXZ和InPz的顺序逐渐变窄，说明羟基四苯咪唑衍生物的电子跃迁能力可通过取代基进行调节。

表 5 TD PBE0/6-31G(d, p)方法获得的吸收光谱、振子强度和主要跃迁组成

Table 5 Absorption spectra, oscillator strengths and main transition configurations obtained by TD PBE0/6-31G(d, p) method

| Compound | Electronic transition | Wavelength /nm | $f$ | Main configuration |
|---|---|---|---|---|
| HPI-TPA | $S_0 \rightarrow S_1$ | 350 (338)[16] | 0.9385 | HOMO−1→LUMO (75.8%)<br>HOMO→LUMO+1 (15.3%) |
| | $S_0 \rightarrow S_2$ | 342 | 0.2341 | HOMO−2→LUMO (11.8%)<br>HOMO→LUMO (77.5%) |
| | $S_0 \rightarrow S_3$ | 340 | 0.1554 | HOMO−2→LUMO (83.4%)<br>HOMO→LUMO (10.0%) |
| HPI-PCz | $S_0 \rightarrow S_1$ | 358 | 0.0043 | HOMO→LUMO (98.7%) |
| | $S_0 \rightarrow S_2$ | 340 (339)[12] | 0.1363 | HOMO−2→LUMO (5.3%)<br>HOMO−1→LUMO (13.5%)<br>HOMO→LUMO+1 (73.5%) |
| | $S_0 \rightarrow S_3$ | 338 | 0.4745 | HOMO−2→LUMO (47.6%)<br>HOMO−1→LUMO (16.0%)<br>HOMO−1→LUMO+1 (12.2%)<br>HOMO→LUMO+1 (18.9%) |
| HPI-DMAC | $S_0 \rightarrow S_1$ | 398 | 0.0007 | HOMO→LUMO (81.3%)<br>HOMO→LUMO+1 (11.5%) |
| | $S_0 \rightarrow S_2$ | 381 | 0.0007 | HOMO−1→LUMO (71.3%)<br>HOMO−1→LUMO+1 (23.4%) |
| | $S_0 \rightarrow S_3$ | 358 | 0.0046 | HOMO−2→LUMO (98.8%) |
| | $S_0 \rightarrow S_{10}$ | 309 | 0.2398 | HOMO−2→LUMO+2 (93.7%) |
| HPI-PTZ | $S_0 \rightarrow S_1$ | 397 | 0.0002 | HOMO→LUMO (72.9%)<br>HOMO→LUMO+1 (21.7%) |
| | $S_0 \rightarrow S_2$ | 393 | 0.0001 | HOMO−1→LUMO (80.3%)<br>HOMO−1→LUMO+1 (12.7%) |
| | $S_0 \rightarrow S_3$ | 363 | 0.0038 | HOMO−2→LUMO (98.9%) |
| | $S_0 \rightarrow S_{10}$ | 310 | 0.1613 | HOMO−2→LUMO+2 (61.1%)<br>HOMO−1→LUMO+2 (28.6%) |
| HPI-PXZ | $S_0 \rightarrow S_1$ | 444 | 0.0186 | HOMO→LUMO (74.1%) |
| | $S_0 \rightarrow S_2$ | 442 | 0.0012 | HOMO−1→LUMO (79.4%)<br>HOMO−1→LUMO+1 (13.8%) |
| | $S_0 \rightarrow S_3$ | 391 | 0.0014 | HOMO→LUMO (16.5%)<br>HOMO→LUMO+1 (81.7%) |
| | $S_0 \rightarrow S_{14}$ | 310 | 0.2415 | HOMO−2→LUMO+2 (92.7%) |
| HPI-InPz | $S_0 \rightarrow S_1$ | 466 | 0.0043 | HOMO→LUMO (77.5%)<br>HOMO→LUMO+1 (18.5%) |
| | $S_0 \rightarrow S_2$ | 462 | 0.0049 | HOMO−1→LUMO (81.9%)<br>HOMO−1→LUMO+1 (12.6%) |
| | $S_0 \rightarrow S_3$ | 411 | 0.0006 | HOMO→LUMO (20.2%)<br>HOMO→LUMO+1 (78.2%) |
| | $S_0 \rightarrow S_9$ | 357 | 0.1086 | HOMO−1→LUMO+3 (11.9%)<br>HOMO−1→LUMO+6 (66.7%) |

表 6 所研究化合物的发射波长、振子强度、主要跃迁轨道和跃迁系数

Table 6 Emission wavelengths, oscillator strengths, main transition orbitals and transition coefficients of studied compounds

| Compound | Wavelength /nm | $f$ | Main configuration |
|---|---|---|---|
| HPI-TPA | 448 (402)[16] | 0.1348 | HOMO→LUMO (96.8%) |
| HPI-PCz | 498 (490)[16] | 0.0022 | HOMO→LUMO (99.5%) |
| HPI-DMAC | 502 | 0 | HOMO→LUMO (96.9%) |
| HPI-PTZ | 605 | 0 | HOMO→LUMO (97.3%) |
| HPI-PXZ | 600 | 0 | HOMO→LUMO (97.0%) |
| HPI-InPz | 643 | 0 | HOMO→LUMO (97.3%) |

## 参 考 文 献


[1] Shirota Y. Organic materials for electronic and optoelectronic devices[J]. Journal of Materials Chemistry, 2000, 10(1): 1-25.

[2] Lai W Y, Zhu R, Fan Q L, et al. Monodisperse six-armed triazatruxenes: microwave-enhanced synthesis and highly efficient pure-deep-blue electroluminescence[J]. Macromolecules, 2006, 39(11): 3707-3709.

[3] Tonzola C J, Kulkarni A P, Gifford A P, et al. Blue-light-emitting oligoquinolines: synthesis, properties, and high-efficiency blue-light-emitting diodes[J]. Advanced Functional Materials, 2007, 17(6): 863-874.

[4] 孙阿辉, 李耀召, 陈果, 等. 基于深蓝光激基复合物构筑的OLED植物照明光源[J]. 光学学报, 2022, 42(4): 0423001.
Sun A H, Li Y Z, Chen G, et al. Organic light-emitting diodes based on deep-blue exciplex for plant growth[J]. Acta Optica Sinica, 2022, 42(4): 0423001.

[5] 季渊, 龚淑萍, 穆廷洲, 等. 基于亮度衰减模型的硅基OLED微显示器寿命研究[J]. 光学学报, 2021, 41(19): 1923003.
Ji Y, Gong S P, Mu T Z, et al. Lifetime of OLED-on-silicon microdisplay based on luminance decay model[J]. Acta Optica Sinica, 2021, 41(19): 1923003.

[6] 付秀华, 陈奕辛, 刘冬梅, 等. 基于Head-Mounted Display补偿VR色温性别差异光学薄膜的研制[J]. 光学学报, 2021, 41(3): 0331001.
Fu X H, Chen Y X, Liu D M, et al. Development of optical films based on head-mounted display to compensate for gender differences in color temperature of VR[J]. Acta Optica Sinica, 2021, 41(3): 0331001.

[7] 潘赛虎, 于航, 赵云平, 等. 金属纳米颗粒的导入对顶发射OLED光取出影响的FDTD模拟与研究[J]. 光学学报, 2022, 42(9): 0916001.
Pan S H, Yu H, Zhao Y P, et al. FDTD simulation and study on effect of metal nanoparticle introduction on light extraction of top-emitting OLED[J]. Acta Optica Sinica, 2022, 42(9): 0916001.

[8] Sasabe H, Kido J. Development of high performance OLEDs for general lighting[J]. Journal of Materials Chemistry C, 2013, 1(9): 1699-1707.

[9] Chen W C, Lee C S, Tong Q X. Blue-emitting organic electrofluorescence materials: progress and prospective[J]. Journal of Materials Chemistry C, 2015, 3(42): 10957-10963.

[10] Thomas K R, Lin J T, Tao Y T, et al. Light-emitting carbazole derivatives: potential electroluminescent materials[J]. Journal of the American Chemical Society, 2001, 123(38): 9404-9411.

[11] Zhang Y F, Cheng G, Zhao Y, et al. Organic pure-blue-light-emitting devices based on terfluorenes compounds[J]. Applied Physics Letters, 2005, 87(24): 241112.

[12] Liu Q D, Lu J, Ding J, et al. Monodisperse starburst oligofluorene-functionalized 4, 4′, 4″-tris(carbazol-9-yl)-triphenylamines: their synthesis and deep-blue fluorescent properties for organic light-emitting diode applications[J]. Advanced Functional Materials, 2007, 17(6): 1028-1036.

[13] Park S, Kwon O H, Kim S, et al. Imidazole-based excited-state intramolecular proton-transfer materials: synthesis and amplified spontaneous emission from a large single crystal[J]. Journal of the American Chemical Society, 2005, 127(28): 10070-10074.

[14] Kajjam A B, Dubey D K, Kumar Yadav R A, et al. Tetraphenylimidazole-based luminophores for explosive chemosensors and OLEDs: experimental and theoretical investigation[J]. Materials Today Chemistry, 2019, 14: 100201.

[15] Dwivedi B K, Singh V D, Kumar Y, et al. Photophysical properties of some novel tetraphenylimidazole derived BODIPY based fluorescent molecular rotors[J]. Dalton Transactions, 2020, 49(2): 438-452.

[16] Li W, Chasing P, Nalaoh P, et al. Hydroxy-tetraphenylimidazole derivatives as efficient blue emissive materials for electroluminescent devices[J]. Chemistry, 2022, 17(14): e202200266.

[17] Gu B, Mi N X, Zhang Y Y, et al. A tetraphenylimidazole-based fluorescent probe for the detection of hydrogen sulfide and its application in living cells[J]. Analytica Chimica Acta, 2015, 879: 85-90.

[18] Song R, Ma Y S, Bi A Y, et al. Highly selective and sensitive detection of arsenite ions(III) using a novel tetraphenylimidazole-based probe[J]. Analytical Methods: Advancing Methods and Applications, 2021, 13(42): 5011-5016.

[19] Aradhyula B P R, Chinta R V R N, Dhanunjayarao K, et al. Synthesis and characterization of poly(tetraphenylimidazole)s and their application in the detection of fluoride ions[J]. RSC Advances, 2020, 10(22): 13149-13154.

[20] Wada Y, Nakagawa H, Matsumoto S, et al. Organic light emitters exhibiting very fast reverse intersystem crossing[J]. Nature Photonics, 2020, 14(10): 643-649.

[21] He Z Z, Cai X Y, Wang Z H, et al. Reversible switching between normal and thermally activated delayed fluorescence towards "smart" and single compound white-light luminescence via controllable conformational distribution[J]. Science China Chemistry, 2018, 61(6): 677-686.

[22] Zhang D W, Teng J M, Wang Y F, et al. D-π*-A type planar chiral TADF materials for efficient circularly polarized electroluminescence[J]. Materials Horizons, 2021, 8(12): 3417-3423.

[23] Yang W, Ning W M, Jungchi H, et al. Polycyclic phenazine-derived rigid donors construct thermally activated delayed fluorescence emitters for highly efficient orange OLEDs with extremely low roll-off[J]. Chemical Engineering Journal, 2022, 438: 135571.

[24] 邹陆一. 多功能有机电致发光材料的理论研究[D]. 长春: 吉林大学, 2009: 1-7.
Zou L Y. Theoretical investigations on the multifunctional organic light-emitting materials[D]. Changchun: Jilin University, 2009: 1-7.

[25] Frisch M J, Trucks G W, Schlegel H B, et al. Gaussian 09, Revision A. 02[D/EB]. [2022-11-08]. http://gaussian.com.

[26] Miehlich B, Savin A, Stoll H, et al. Results obtained with the

correlation energy density functionals of becke and Lee, Yang and Parr[J]. Chemical Physics Letters, 1989, 157(3): 200-206.
[27] Perdew J P, Burke K, Ernzerhof M. Generalized gradient approximation made simple[J]. Physical Review Letters, 1996, 77(18): 3865-3868.
[28] Yanai T, Tew D P, Handy N C. A new hybrid exchange-correlation functional using the Coulomb-attenuating method (CAM-B3LYP)[J]. Chemical Physics Letters, 2004, 393: 51-57.
[29] Han J H, Liu X C, Sun C F, et al. Ingenious modification of molecular structure effectively regulates excited-state intramolecular proton and charge transfer: a theoretical study based on 3-hydroxyflavone[J]. RSC Advances, 2018, 8(52): 29589-29597.
[30] Johnee Britto N, Panneerselvam M, Deepan Kumar M, et al. Substituent effect on the photophysics and ESIPT mechanism of *N*,*N*′-bis(salicylidene)-*p*-phenylenediamine: a DFT/TD-DFT analysis[J]. Journal of Chemical Information and Modeling, 2021, 61(4): 1825-1839.
[31] Tripathi A, Prabhakar C. Optoelectronic and charge-transport properties of truxene, isotruxene, and its heteroatomic (N, O, Si, and S) analogs: a DFT study[J]. Journal of Physical Organic Chemistry, 2019, 32(6): e3944.
[32] Ren X F, Ren A M, Feng J K, et al. A density functional theory study on photophysical properties of red light-emitting materials: meso-substituted porphyrins[J]. Journal of Photochemistry and Photobiology A: Chemistry, 2009, 203(2/3): 92-99.
[33] Liu Y L, Feng J K, Ren A M. Theoretical study of optical and electronic properties of the bis-dipolar diphenylamino-endcapped oligoarylfluorenes as promising light emitting materials[J]. Journal of Physical Organic Chemistry, 2007, 20(8): 600-609.
[34] Li X B, Wang X Y, Gao J W, et al. Theoretical study on a multifunctional electroluminescent molecule $Mes_2B$[*p*-4,4′-biphenyl-Nph(1-naphthyl)] [J]. Chemical Physics, 2006, 326(2/3): 390-394.

# Theoretical Investigation of Hole and Electron Transport Properties for Hydroxy-Tetraphenylimidazole Derivatives

Liao Fan[1], Cui Xiaoying[2], Min Chungang[2*], Ren Aimin[3**]

[1]*Faculty of Materials Science and Engineering, Kunming University of Science and Technology, Kunming* 650093, *Yunnan, China*;

[2]*Research Center for Analysis and Measurement, Kunming University of Science and Technology, Kunming* 650093, *Yunnan, China*;

[3]*Institute of Theoretical Chemistry, College of Chemistry, Jilin University, Changchun* 130021, *Jilin, China*

## Abstract

**Objective** Organic light-emitting diode (OLED) technology has attracted extensive attention due to its increasing demand in the fields of full-color flat-panel display and lighting. In general, the primary colors, i. e., red, green, and blue, are required for full-color display or white OLED (including solid-state lighting). In particular, the material that can emit blue light plays an important role in color temperature management and the color rendering index. Therefore, many studies on new blue light materials have been conducted for higher efficiency and better performance. In recent years, a new class of imidazolyl materials, hydroxyl-substituted tetraphenylimidazole (HPI) and its analogs, have attracted more and more attention because they can be used not only as a blue light material but also as a probe to detect hydrogen sulfide, arsenite ions, and fluoride ions. In this paper, the electron donor substituents, 9, 9-dimethyl-9, 10-dihydroacridine (DMAC), triphenylamine (TPA), 10H-phenothiazine (PTZ), 10H-phenoxazine (PXZ), phenyl carbazole (PCz), and 5H-indole [3, 2, 1-de] phenazine (InPz) are used to disubstitute the 3, 5 positions of *N*-phenyl of hydroxy-tetraphenylimidazole. As a result, six hydroxy-tetraphenylimidazole derivatives are obtained. After that, their electronic structures and photophysical properties are studied with density-functional theory (DFT) and time-dependent density-functional theory (TDDFT). In addition, as the compounds containing electron-rich groups, such as triphenylamine and carbazole, are often used as hole transport materials, we also investigate the possibility of the six derivatives as hole and electron transport materials.

**Methods** The first step is to verify the accuracy of functionals. Specifically, B3LYP, PBE0, and CAM-B3LYP functionals combined with the 6-31G(d, p) basis set are used to optimize the ground-state and the first single-excited-state geometries of experimentally synthesized HPI-TPA and HPI-PCz. The absorption and emission spectra are calculated. For HPI-TPA and HPI-PCz, the calculated results obtained by B3LYP and CAM-B3LYP functionals are significantly different from the experimental values, while those obtained by PBE0 are close to the experimental values. The same trends are reflected in emission spectra. Therefore, the PBE0 functional is used in the subsequent calculations. Then, the PBE0 functional combined with the 6-31G(d, p) basis set is used to optimize the geometries of the six hydroxy-

tetraphenylimidazole derivatives. Given the optimized geometry, the ionization potentials (IP), electron affinity potentials (EA), hole extraction potentials (HEP), electron extraction potentials (EEP), hole reorganization energy $\lambda_{hole}$, and electron reorganization energy $\lambda_{electron}$ can be calculated. Finally, the excited-state geometries of the six derivatives are optimized by the TD PBE0/6-31G(d, p) method, and the absorption and emission spectra of the studied molecules are calculated by the same method.

**Results and Discussions** According to the Kohn-Sham frontier orbitals and the contribution of electron density for HPI-TPA, HPI-PTZ, HPI-PXZ, and HPI-InPz, the electron clouds of the highest occupied molecular orbits (HOMOs) are mainly located on the R-down group, and the HPI and R-up groups almost do not contribute to HOMOs. For HPI-PCz, the contribution of the HPI group to HOMOs is 99.3%, while the contributions of the R-up and R-down groups are almost zero. For HPI-DMAC, the contribution of the R-up group to HOMOs is 100.0%, while the contributions of the HPI and R-down groups are zero. In contrast, for HPI-TPA, HPI-PTZ, HPI-PXZ, and HPI-InPz, the contributions of the R-down group decrease from 98.8%, 100.0%, 99.9%, and 100.0% in HOMOs to 42.7%, 22.1%, 23.0%, and 23.4% in lowest unoccupied molecular orbits (LUMOs), respectively. For HPI-PCz, the contribution of HPI decreases from 99.3% in HOMO to 53.4% in LUMO. For HPI-DMAC, the contribution of the R-up group decreases from 100.0% in HOMO to 24.5% in LUMO. This shows that there is a lot of electron transfer from HOMO to LUMO. In addition, the results of HOMO energies, LUMO energies, HOMO-LUMO gaps, ionization potentials, and electron affinities demonstrate that HPI-TPA, HPI-DMAC, HPI-PTZ, HPI-PXZ, and HPI-InPz show good hole transport ability, and HPI-PTZ, HPI-PXZ, and HPI-InPz also show good electron injection ability. Moreover, it is found that the HOMO-LUMO energy gaps of the studied compounds gradually narrow along the order of TPA, PCz, DMAC, PTZ, PXZ, and InPz. This indicates that the electronic transition ability of hydroxy-tetraphenylimidazole derivatives can be regulated by substituents. The absorption and emission spectra show that for HPI-DMAC, HPI-PTZ, HPI-PXZ, and HPI-InPz, the $S_1 \rightarrow S_0$ electronic transition is forbidden because the oscillator strengths are almost zero. HPI-TPA and HPI-PCz can emit bright blue light.

**Conclusions** In this paper, the photophysical properties of six disubstituted hydroxy-tetraphenylimidazole derivatives are studied by the TD PBE0/6-31G(d, p) method. The results show that there is a lot of electron transfer in all molecules during the transition from HOMO to LUMO. HPI-PTZ, HPI-PXZ, and HPI-InPZ have strong hole and electron injection abilities. The HOMO-LUMO energy gaps gradually narrow along the order of TPA, PCz, DMAC, PTZ, PXZ, and InPz. This indicates that the electronic transition capacity of hydroxy-tetraphenylimidazole derivatives can be regulated by substituents.

**Key words** spectroscopy; hole and electron transport; disubstituted hydroxy-tetraphenylimidazole derivatives; fluorescence; density functional theory